MÖSSBAUER MINERALOGY ON THE MOON: THE LUNAR REGOLITH

Richard V. MORRIS[1], Göstar KLINGELHÖFER[2], Randy L. KOROTEV[3], and Tad D. SHELFER[4]

[1]Code SN3 NASA Johnson Space Center, Houston, TX 77058, USA

[2]Darmstadt University of Technology, Schlossgartenstr. 9, 64289, Germany

[3]Department of Earth and Planetary Sciences, Washington University, St. Louis, MO 63130, USA

[4]Viking Science & Technology Inc., 16821 Buccaneer Ln., Houston, TX 77058, USA

(Submitted to *Hyperfine Interactions*, Oct. 1997)

Abstract. A first-order requirement for spacecraft missions that land on solid planetary objects is instrumentation for mineralogical analyses. For purposes of providing diagnostic information about naturally-occurring materials, the element iron is particularly important because it is abundant and multivalent. Knowledge of the oxidation state of iron and its distribution among iron-bearing mineralogies tightly constrains the types of materials present and provides information about formation and modification (weathering) processes. Because Mössbauer spectroscopy is sensitive to both the valence of iron and its local chemical environment, the technique is unique in providing information about both the relative abundance of iron-bearing phases and oxidation state of the iron. The Mössbauer mineralogy of lunar regolith samples (primarily soils from the Apollo 16 and 17 missions to the Moon) were measured in the laboratory to demonstrate the strength of the technique for in situ mineralogical exploration of the Moon. The regolith samples were modeled as mixtures of five iron-bearing phases: olivine, pyroxene, glass, ilmenite, and metal. Based on differences in relative proportions of iron associated with these phases, volcanic ash regolith can be distinguished from impact-derived regolith, impact-derived soils of different geologic affinity (e.g., highlands, maria) can be distinguished on the basis of their constituent minerals, and soil maturity can be estimated. The total resonant absorption area of the Mössbauer spectrum can be used to estimate total FeO concentrations.

Introduction

A first-order requirement of spacecraft missions that land on solid planetary objects such as the Moon, Mars, and asteroids is instrumentation for in situ mineralogical and elemental analyses. Such analyses provide the data needed for primary classification and characterization of surface materials present and, by inference, the processes that formed and subsequently modified them. For purposes of providing diagnostic information about naturally occurring materials, the element iron is particularly important because it is abundant and multivalent (primarily 0, +2, and +3 oxidation states). Knowledge of

the oxidation state of iron and its distribution among iron-bearing minerals constrains the types of materials present. For example, different rock types are characterized by different assemblages of the iron-bearing silicate (e.g., olivine and pyroxene) and oxide (e.g., ilmenite and magnetite) minerals. The distribution of iron oxidation states provides information about redox conditions during igneous, metamorphic, and sedimentary petrogenetic processes. There are often differences in the ratios of iron oxidation states between primary and secondary minerals produced by weathering and alteration. These ratios and the mineralogy of secondary minerals provide information on the nature and extent of weathering and alteration processes. The pivotal role of iron for planetary exploration was recognized by *COMPLEX* [1], which recommended development of flight instruments that would identify the mineralogy and the oxidation state of iron in planetary surface materials. This recommendation was a result of the Viking missions to Mars which, although highly successful, did not have instrumentation specifically sensitive to mineralogy.

Because iron Mössbauer spectroscopy is sensitive to both the oxidation state and local chemical environment of ^{57}Fe (2.2% natural abundance), it provides quantitative data on the relative distribution of iron according to both oxidation state and mineralogy. The technique is thus ideally positioned for meeting planetary exploration goals relating to the mineralogy and oxidation state of iron. Mössbauer instruments suitable for deployment by landers or rovers on planetary surfaces exist as flight prototypes [2, 3] and have been proposed by the authors for planetary surface missions to the Moon and Mars. Development of planetary Mössbauer instruments has created an imperative to understand the Mössbauer mineralogy of extraterrestrial samples (lunar samples and meteorites, including those from Mars) and planetary surface analogues for the purpose of developing a basis for interpretation of in situ measurements.

By "Mössbauer mineralogy", we mean (1) the identification of iron bearing phases from peak positions in Mössbauer spectra and (2) the quantitative distribution of iron among phases or according to oxidation state based on areas of peaks in the spectra. Absolute abundances of iron-bearing phases are not obtainable unless total-sample and individual-phase iron concentrations are known from independent measurements. In some cases, e.g., hematite (α-Fe_2O_3), ilmenite ($FeTiO_3$), and metallic iron (Fe^0), but not

others, e.g., olivine ($(Mg,Fe^{2+})SiO_4$), pyroxene ($(Ca,Mg,Fe^{2+})SiO_3$), and glass, the iron content of a phase can be inferred from its mineralogy.

In this paper, we focus on lunar Mössbauer mineralogy, its relationship to other kinds of mineralogical data, and its utility as a method for mineralogical exploration of the Moon. Our data are primarily for samples of lunar regolith fines ("soils"), but we also report some data for rocks. Previous Mössbauer studies of lunar samples are largely from the early to mid 1970's when lunar samples were being returned from the Moon as a part of the Apollo program [e.g., 4-11]. Since then, more conventional geological techniques (e.g., optical petrography, electron probe microanalysis, and scanning electron microscopy) have dominated mineralogical studies of lunar samples [e.g., 12-14].

Brief Overview of Lunar Mineralogy and Geology

In large part because of the absence of water and the extremely reducing conditions, lunar mineralogy is relatively simple: the crust of the Moon consists mainly of plagioclase feldspar, pyroxenes, olivine, ilmenite, and glass. Iron is present as Fe^{2+} in silicate, oxide, and minor sulfide phases and as Fe^0 in Fe and Fe-Ni metal alloys; Fe^{3+} is essentially absent. The impact of giant meteoroids early in lunar history excavated huge cavities and the lunar maria ("seas") were formed by the subsequent filling of those basins by lavas. Thus, lunar rocks generally have one of two affinities: those from the ancient, heavily-cratered highlands, or those from the younger maria. There are two types of volcanic material in and near the maria: crystalline rock known as mare basalt, and volcanic (pyroclastic) ash that is mainly glassy. Mare basalt and volcanic glass are both rich in iron (19–22% as FeO) which leads to the low albedo of the maria. Most rocks from the highlands are dominated by plagioclase and thus have a low abundance of Fe-bearing minerals. The average concentration of FeO in the highlands is consequently low (4–5%) and the albedo is high. A component of the ejecta of at least some basins was impact-melt breccia that is substantially richer in iron (8–11% FeO) than typical highlands crust. These mafic impact-melt breccias are probably rare

components of the highlands overall, but because the six Apollo missions that retrieved samples all landed in or near major impact basins, mafic melt breccias are a common component of Apollo samples.

Lunar regolith (soil) is largely the result of repetitive meteoritic impact, although some deposits of volcanic ash are present.. Because of the mixing effect of countless meteorite impacts, any given sample of soil contains material from both the highlands and the maria. However, impact mixing is inefficient, so that soil formed on the maria, for example, still consists mainly of mare basalt. In most lunar soils, a large fraction of the originally crystalline material has been converted to glass by impact melting.

More detailed accounts of lunar mineralogy and geology can be found in Papike et al. [13], Heiken et al. [14], Taylor [15, 16], and references therein.

Methodology of Mössbauer Mineralogy

Samples and Sample Analysis

Samples of lunar soil were selected from each of the six Apollo missions that collected samples from the Moon to cover the range of available composition and mineralogy. Each soil sample has a 5-digit number that includes identifiers for the mission number. Soil samples from the Apollo 11 (10084), Apollo 12 (120xx), and Apollo 15 (15013) missions and several soil samples from the Apollo 17 (7xxx1) mission were formed mainly from mare basalt. Three samples from these missions (15421, 74001, and 74220) consist mainly of volcanic ash. The feldspathic lunar highlands are represented by soils from the Apollo 16 (6xxx1) mission; some soils from Apollo 17 also contain feldspathic highland material. Soils from Apollo 14 (e.g., 14148) formed largely (>80%) from mafic impact-melt breccias. Most soils from Apollo 16 and some from Apollo 17 also contain a significant component (30-60%) of mafic impact-melt breccia.

Samples of lunar soil (<1 mm and <20 μm sieve fractions) and rock (powders) were analyzed in transmission geometry on a Ranger MS-1200 Mössbauer spectrometer configured in a vertical orientation so that particulate samples (200 to 250 mg) could be conveniently analyzed. In the Mössbauer experiment,

absorbers are normally prepared by grinding samples to fine powders and dispersing them in inert and iron-free materials (e.g., wax or epoxy) in order to approximate conditions of a uniform absorber, which is a requirement for quantitative determination of phase abundances from peak areas [e.g., 17]. Our lunar soils could not be ground because the process destroys their integrity for other types of analysis. For the same reason, we were not able to mix lunar samples with inert materials. In addition, sample preparation procedures like grinding would be a highly undesirable requirement (too complex an operation) for robotic exploration of the Moon by Mössbauer spectroscopy. Part of the purpose of this paper is to document how well the method can do with no sample preparation. Samples were placed in 1.8-cm-diameter polypropylene cups to a uniform depth. Average absorber thicknesses were ~100 mg/cm^2 of sample or 4-16 mg/cm^2 of natural Fe (calculated using a range of 5–20 wt% FeO for lunar soils). Because of sample granularity, actual thickness varied from point to point depending on the particles actually present.

Because one of the goals of Mössbauer mineralogy on the lunar surface is to obtain quantitative data on the abundances of iron bearing phases, it is appropriate to discuss, in more detail, the consequences of non-uniform (granular) absorbers. In a uniform absorber, discrete particles of each individual phase in a powder are small compared to the sample thickness and are homogeneously dispersed throughout its volume so that the nature of the optical path of the γ-rays through the absorber is invariant with respect to its incidence location [e.g., 17-19]. Because the grain-size fraction we analyze (typically <1 mm) is comparable to the physical sample thickness (typically ~1–2 mm), absorber granularity is present. It is possible, for example, that all the ilmenite in a particular sample is heterogeneously distributed as a small number of ~750 nm particles. Because of the non-linear resonance-versus-thickness behavior [e.g., 18], this would cause the observed peak areas to be less than if the ilmenite were present as extremely fine particles. A specific example is given by Williamson et al. [19], who show Mössbauer spectra for two particulate pyrite absorbers with the same average absorber thickness (~20 mg/cm^2) and different average particle diameters. The peak area of the pyrite absorber with 19 μm particles was a factor of 2.6 larger

than that for the absorber with 125 μm particles. Similarly, a multicomponent absorber, whose components all have identical thickness with respect to iron but much different average particle diameters, will have a Mössbauer spectrum in which the component areas, rather than being equal, increase with decreasing particle diameter. Williamson et al. [19] describe a sample of coal in which the relative areas of the iron-bearing components (pyrite, a carbonate, and a sulfate) dramatically changed by grinding the sample. Another effect of granularity is mass absorption [e.g., 18]. Large plagioclase grains can (through mass absorption) shield smaller iron-bearing grains with the result that their area is underrepresented in the Mössbauer spectrum. With large particles, it is also possible to have polarization effects from non-random orientations of mineral grains [e.g., 18]. As demonstrated below, however, if such factors influenced our measurements, they were not strong influences. A possible mitigating factor is that for Apollo 17 soils, for example, ~70% of the material in the <1 mm grain-size fraction of a typical sample also passes through a 90 μm sieve [20].

Iron-Bearing Components and Mössbauer Spectra

Previous Mössbauer and petrographic studies [e.g., 4, 12, 13] have established that the major iron-bearing phases in lunar samples are pyroxene (Px: $(Ca,Mg,Fe^{2+})SiO_3$), ilmenite (Ilm: $(Mg,Fe^{2+})TiO_3$), olivine (Ol: $(Mg,Fe^{2+})_2SiO_4$), glass (Gl: amorphous silicate Fe^{2+}), and metallic iron and/or iron-nickel alloys (α-Fe^0). Less abundant iron-bearing phases which may be important for certain samples include trolite ($Fe^{2+}S$), armalcolite $(Mg,Fe^{2+})Ti_2O_5$, chromite $((Fe^{2+},Mg)Cr_2O_4)$, ulvospinel $((Fe^{2+})_2TiO_4)$, and spinel $((Mg,Fe^{2+})Al_2O_4$. Strictly speaking, the mineral names ilmenite, chromite, and spinel imply the compositions $FeTiO_3$, $FeCr_2O_4$, and $MgAl_2O_4$, respectively. We use generalized formulas to indicate that the compositions are usually not exactly stoichiometric. Glass occurs in lunar regolith both as products of impact melting and volcanism. Representative Mössbauer spectra of impact-derived regoliths from each of the six Apollo missions are shown in Figure 1. Spectra for regoliths formed predominantly from volcanic

ash (glass) are shown in Figure 2. Even from visual inspection of the spectra, it is apparent that impact-derived regoliths are mixtures in variable proportions of olivine, pyroxene, glass, and ilmenite and that volcanic ash soils are mostly glass and olivine. A few peaks of the α-Fe^0 sextet are also clearly visible in a few of the spectra.

Mössbauer Parameters and Least-Squares Fitting Procedure

Mössbauer spectra were fit by a least-squares procedure to theoretical line shapes using an in-house computer program (JSCFIT). Derived Mössbauer parameters relating to identification of individual phases are the isomer shift (IS), quadrupole shift (QS), and magnetic hyperfine field (B_{hf}). The IS is referenced to metallic iron foil at room temperature. For sextets, QS and B_{hf} are calculated from 1/2([6-5]-[2-1]) and [6-1], where the numbers inside the square brackets are peak centers numbered from lowest to highest velocity. The percentage of total peak area for particular iron-bearing phases is equal to the percentage of the total iron in the sample (atomic %) that is incorporated in that phase, assuming Debye Waller factors [e.g., 21] are all the same and that the absorber is uniform. In order to distinguish measurements of the distribution of Fe among phases from other measurements of mineralogy (e.g., modal petrography), we will adopt a notation with brackets around abbreviations for the phase name for phase abundances from Mössbauer mineralogy. Thus, "{Ol}" denotes the percentage of total iron (atomic %) associated with the mineral olivine in a sample, and "Ol" would denote the concentration of olivine (usually as a wt %). Thus, it is possible for a sample to have {Ol}=0% and Ol=100% if it were pure olivine that contained no iron (e.g., Mg_2SiO_4). Similarly, Fe_2SiO_4 would have {Ol}=100% and Ol=100%.

To fit the Mössbauer spectra of lunar samples to theoretical lineshapes, we used a model with six iron-bearing phases having a total of 17 individual peaks: olivine (doublet), M1 and M2 sites of pyroxene (two doublets), glass (doublet), ilmenite (doublet), α-Fe^0 (sextet), and nanophase (superparamagnetic) Fe^0 (singlet). In addition, there is a weak singlet from Fe impurities in the Al metal sample holder and the Be

metal window of the proportional counter detector. In experiments with no sample, the position and width of the singlet were determined to be 0.218 and 0.540 mm/s, respectively. Values for peak centers and widths for a generic lunar soil (for use as initial values for fitting an arbitrary lunar sample) were determined by obtaining the best aggregate fit for a series of samples that have the highest proportions of the individual components. The selected samples were 73131 and 74001 (olivine), 67511 (pyroxene, M1 and M2 sites), 10084 and 71061 (ilmenite), 15421 and 74220 (glass), and 10084 and 60501 (α-Fe^0). The Mössbauer spectra of these soils are shown in Figures 1 and 2. The <20 μm sieve fraction of lunar soil 10084 was used for nanophase Fe^0. A significant number of parameter constraints were required to obtain the best aggregate fit for these samples. As discussed next, the basic idea was to constrain the peak parameters for all but the most intense components to initial values.

All peak shapes were Lorentzians except for the glass doublet for which the shape was allowed to vary between Lorentzian and Gaussian. Peak area ratios were always constrained to 1:1 for doublets and to 3:2:1:1:2:3 for the α-Fe^0 sextet. For 73131 and 74001, peak positions and widths for olivine were unconstrained and constrained equal, respectively, and the remaining peak centers and widths were constrained to initial values. For 67511, peak positions of the pyroxene M2 doublet were unconstrained and the peak widths for the four pyroxene lines (from M2 and M1 doublets) were constrained to be equal. Peak centers for the M1 doublet were constrained by requiring its value of IS to be 0.02 mm/s more positive than that for the M2 doublet. The remaining peak parameters were constrained to initial values. The low intensity of the M1 doublet required its centers be constrained as described; the difference in the values of IS for the M1 and M2 doublets is consistent with the difference measured for pyroxene mineral separates of lunar soils [e.g., 4]. For 10084 and 71061, peak positions and widths for ilmenite were unconstrained and constrained equal, respectively, and the remaining parameters were constrained to initial values. For 15421 and 74220, peak centers, widths, and fraction Gaussian shape for glass were unconstrained, and the remaining peak centers and widths were constrained to initial values. For 10084

and 60501, peak centers for lines 1, 2, 5, and 6 of the α-Fe^0 sextet were unconstrained, and the widths of lines 1 and 2 were constrained equal to those of 6 and 5, respectively. The centers of peaks 3 and 4 were constrained by the positions of the other four peaks and -0.5711 as the value for the ratio of excited to ground state gyromagnetic ratios. For 10084 (<20 μm), the peak center and width for the np-Fe^0 were the only peak parameters that were not constrained. We found that the singlet for np-Fe^0 was not distinguishable from the one for impurity Fe in the Al and Be sample holder and detector window. Therefore, we did all of our fits with a single peak for iron in these three sites for Fe and then corrected for the contribution of the "blank" to the peak area. After these fits were done, the resulting peak parameters were used as initial values, and the process described above was repeated. After three more repetitions, the initial and calculated peak parameters did not differ significantly (within ±0.004 mm/s). These parameters characterize our generic lunar soil, and they are compiled in Table 1.

The fitting procedure for an arbitrary lunar soil was to use the peaks parameters in Table 1 as initial parameter values and a three-pass process in which each pass involved fewer constraints. (1) All peak centers and widths are constrained to initial values. Areas for all doublets are constrained to 1:1 and the areas of the α-Fe^0 sextet constrained to 3:2:1:1:2:3. (2) If the areas of the olivine, ilmenite, and/or M2-pyroxene doublets are individually >20%, the constraints for their peak centers are released and the widths for each component constrained equal. The peak centers for the pyroxene M1 doublet are constrained as described above for the generic soil. (Note that the widths for the pyroxene M2 and M1 doublets are always constrained to be the same.) In lunar samples, the areas of the olivine, ilmenite, and M2-pyroxene doublets are never all >20% in the same sample. Commonly, peak areas of either olivine and M2-pyroxene doublets or ilmenite and M2-pyroxene doublets are >20% at the same time. (3) If the area of the α-Fe^0 sextet is >5%, the constraints for the centers of peaks 1, 2, 5, and 6 are released and the centers of peaks 3 and 4 constrained by using the value of -0.5711 for the ratio of excited to ground state gyromagnetic ratios. In addition, the widths of peaks 1 and 6 and peaks 2 and 5 are constrained equal. Note that peak centers

for the pyroxene M1 doublet are always constrained with respect to the M2 doublet and that the peak and width constraints on the glass doublet and np-Fe^0 singlet are never released. If they are released, the least-squares fit either does not converge to a solution or gives unrealistic parameter values (e.g., negative phase abundance). The reason this happens is that the low velocity peaks for the pyroxene doublets and the np-Fe^0 singlet strongly overlap (Table 1). It is possible that these constraints on the glass and pyroxene doublets cause solutions to the fit that do not correspond to the actual distribution of Fe^{2+} between pyroxene and glass in the samples. This is a very likely situation because pyroxene mineralogy within a given soil can be highly variable so that the distribution of ferrous sites for pyroxene could mimic the distribution of ferrous sites in glass. The degree to which the Mössbauer method can differentiate ferrous iron in glass and pyroxene is considered later.

Values of IS and QS calculated for phases for which peak centers were not constrained are listed in Table 2. The relative peak areas for individual phases (i.e., percentage of iron associated with individual phases) are compiled in Table 3, and they are equal to the percentage of iron in those phases, provided that the absorbers are sufficiently uniform and the Debye-Waller factors for iron in each phase are approximately equal.

Mössbauer Mineralogy of Lunar Regolith Samples

Pyroxene Versus Glass

As discussed above, the similarity of peak centers and widths for pyroxene (particularly the M2 doublet) and glass could result in fits that are not realistically descriptive of the actual partitioning of iron between pyroxene and glass. A way to evaluate this potential source of error is to consider independent evidence for the abundance of pyroxene and glass. Figure 3 is a plot of {Ol+Gl} versus {Px/(Px+Gl)} for all samples we studied ({Px}={PxM2+PxM1}). Note that all regolith samples studied have greater than 40% {Ol+Gl} and that the ratio {Px/(Px+Gl)} varies over the entire possible range, although the ratio for

most regolith samples is between 0.3 and 0.6. The three samples (15421, 74220, and 74001,119) that have {Px/(Px+Gl)}<0.05 each consist almost entirely of volcanic ash formed during fire-fountaining of low viscosity magmas on the Moon [e.g., 14, 22]. Regolith samples such as these that consist predominantly of volcanic ash are rare in the Apollo sample collection. Petrographic studies show that sample 15421 and 74220 are mostly small (mean grain size: 40 μm for 74220) gray/green and orange glass beads, respectively, but that olivine is present as phenocrysts in the glass [23]. Sample 74001,119 is equivalent to 74220 except that the beads are black because the glass has largely devitrified to crystalline phases [22]. Petrographic studies indicate that the pyroxene abundance is low in these ash samples. Thus, the low pyroxene and high glass-plus-olivine contents of these three samples based on their Mössbauer mineralogy is confirmed by petrographic observations.

Six of the eight samples in Figure 3 that have {Px/(Px+Gl)}>0.75 are powdered rocks. As documented by Ryder and Norman [24], Neal and Taylor [25, 26], and Meyer [27], petrographic studies of 70035 and 75075 (high-Ti mare basalts), 76015 (impact melt breccia), 77017 (anorthositic norite), and 77135 (impact melt breccia) do not indicate the presence of glass. The low abundance of glass ({Gl}<3%) in the crystalline rocks 67215, 76015, 77017, and 77135 based on Mössbauer mineralogy is thus consistent with petrographic observations. Mössbauer results for basalts 70035 and 75075 indicate a higher glass abundance ({Gl}˜12%) than is consistent with petrographic observations (Gl˜0%). It is possible that another iron-bearing phase is present and is being interpreted as glass in our model or (as discussed above) a distribution of sites is present in pyroxene and being interpreted as glass. It is also possible that glass is actually present (as glassy mesostasis), but at too small a scale to be detected by petrographic observations.

In summary, our fitting procedure gives physically reasonable results for relative abundances of glass and pyroxene when applied to samples that are known to consist mostly of either glass or pyroxene from petrographic observations. It is desirable to test the fitting procedure against lunar soils that have, from independent data, comparable levels of {Px} and {Gl}, but we do not know of such a sample.

Volcanic Ash versus Impact-Derived Regoliths

Regoliths formed predominantly of volcanic ash are readily distinguished from those derived predominantly from impact processes (Figure 3) by Mössbauer mineralogy. As discussed above, volcanic ash is characterized by high proportions of glass plus olivine and low proportions of pyroxene; thus measured values of {Ol+Gl} are high (>75%) and {Px/(Px+Gl)} are low (<0.15). Regolith formed predominantly by the comminution and melting accompanying the impact of meteorites are complex mixtures of mineral fragments and glass [e.g., 13, 28] and thus have values of {Px/(Px+Gl)} intermediate to volcanic glass and rocks.

Ilmenite: Mössbauer Mineralogy versus TiO_2 Concentrations

Of the three major iron-bearing minerals in lunar samples (olivine, pyroxene, and ilmenite), only ilmenite contains Ti as a major constituent. Thus, in principle, an independent estimate of the ilmenite abundance of a soil can be calculated from its Ti concentration. In practice, however, such a comparison is not straightforward, as the following analysis indicates. Figure 4 is a plot of measured (i.e., Mössbauer) {Ilm} versus values of {Ilm} calculated from two different models. For Model 1 (squares), calculated values of {Ilm} were obtained simply from chemical concentrations (in atomic %) of Ti and Fe assuming (1) ilmenite is stoichiometric $FeTiO_3$ and (2) that all Ti in the sample occurs in ilmenite (i.e., {Ilm} = (Ti/Fe) × 100%, where Ti and Fe represent the number of moles of the two elements in a given mass of sample). The figure shows that values of {Ilm} calculated from Model 1 are a factor of 2–4 larger than values obtained by Mössbauer mineralogy. This discrepancy might imply that the measured values of {Ilm} are erroneously low for some reason, e.g., the samples are non-uniform absorbers with respect to ilmenite, as discussed in the section on sample analysis. However, Model 1 is overly simplistic and provides only upper limits on the values of {Ilm}. Below we show that the actual concentrations of

ilmenite in the soils are considerably lower than predicted by Model 1 because both assumptions discussed above lead to overestimates of "calculated" values of {Ilm}.

First, lunar ilmenites are not stoichiometric, being deficient in Fe and in extreme cases having compositions approximating $(Mg_{0.2}Fe_{0.8}Ti)O_3$ [e.g., 29-31]. Using this stoichiometry for ilmenite will reduce the calculated values by a factor of 0.8. Second, substantial amounts of Ti are carried by pyroxene (particularly in high-Ti mare basalts) and glass. It is not uncommon for such pyroxene to have Fe/(Fe+Ti) ~ 0.8 (atomic ratio) [e.g., 29-31]. However, the most important reservoir for Ti outside of ilmenite is glass. Volcanic-ash and impact-derived regoliths have values of {Gl} up to 90% and 50%, respectively (Table 2). In impact-produced regoliths, most glass occurs in particles called agglutinates, which are glassy impact melts formed from pre-existing regolith during micrometeorite impact. Agglutinates constitute up to ~50% by number in size separates of lunar soils [e.g., 12, 13]. Because agglutinate glass is formed by melting soil, there is no reason to expect that the Fe/Ti ratio of the glass differs significantly from that for the whole soil.

Model 2 (filled circles) in Figure 4 is the result of calculating {Ilm} using the Fe-deficient stoichiometry for ilmenite and reducing the amount of Ti available for ilmenite formation in accordance with values of {Px} and {Gl} (Table 2), i.e., $\{Ilm\}=0.8(Ti/Fe)(100-\{Gl\}-0.2\{Px\})$. In a glass-rich sample like 74220 ({Gl}=76%), the correction for glass accounts for 80% of the difference between Models 1 and 2 (Figure 4). Considering that the Ti content of both pyroxene and ilmenite likely varies from soil to soil and that there are minor Ti-bearing phases not considered, we consider the agreement between measured and calculated values of {Ilm} for Model 2 to be good. Importantly, with Model 2 there is no longer any evidence for underestimation of {Ilm}, as might be expected if the absorbers are non-uniform with respect to ilmenite, as discussed above.

Comparisons of measured and calculated values of {Ilm} show that (1) Mössbauer spectroscopy can be used to obtain reasonable estimates for the amount of Fe associated with ilmenite in lunar soils and

(2) on average, only one-quarter to one-half of the Ti in impact-derived lunar soil is associated with ilmenite; the rest is in glass, pyroxene, and possibly other mineral phases.

Metallic Iron: Mössbauer Mineralogy versus Magnetics

Values of {tot-Fe^0} in Table 2 can be compared with values of the same parameter calculated from the formula $(\text{tot-Fe}^0)_{mag}/Fe_{chem}$. The numerator is the magnetically-determined total Fe^0 concentration (in units of wt % of sample), and the denominator is the chemically-determined total Fe concentration (in units of wt % of sample). The pertinent magnetic and chemical data are compiled in [32], and the observed and calculated values of {tot-Fe^0} are compared in Figure 5. The agreement is good, as shown by the close correspondence of the data to the 1:1 line.

Total Resonant Absorption Area and FeO Concentration

The total resonant absorption in a Mössbauer spectrum (i.e., the sum over all absorption lines) is proportional to the total amount of ^{57}Fe in the γ-ray beam (in units of g/cm^2). The concentration of ^{57}Fe in the beam is proportional to both sample mass in the beam and concentration of Fe in the sample. Thus, for a series of samples having different FeO concentrations, the total resonant absorption area normalized to sample concentration (in g/cm^2) should be proportional to the FeO concentration in the sample, assuming the absorbers are sufficiently uniform and that the Debye-Waller factors for iron are all approximately equal. Figure 6 shows that this is, in fact, the case for the lunar regolith samples in Table 2. Mössbauer spectroscopy is not the technique of choice for measurements of FeO concentrations, but Figure 6 shows the technique can be used to estimate FeO values in the absence of alternative methods.

Olivine, Pyroxene, and Ilmenite Systematics

We demonstrated above that we have reasonably separated the contributions of ferrous iron to pyroxene and glass and that our samples are sufficiently uniform that we can equate Mössbauer peak areas

(Table 2) with percentages of total iron in particular phases. If sample nonuniformity were an important source of error, the reasonable agreement observed between measured and calculated (from independent data) values of both {Ilm} (Figure 4) and {tot-Fe^0} (Figure 5) would not have been obtained, and the plot of total resonant area versus FeO (Figure 6) would have been nonlinear. Effects of nonuniformity are undoubtedly present, but the observation is that they are small compared to variations in phase abundance. With the validity of the data in Table 2 demonstrated, we discuss next how geologic inferences can be made from the variation in abundances of the major rock-forming minerals among samples of impact-derived regoliths.

If we assume that the glass in these samples is derived predominantly from impact melting of whole soil and that no mineral component was preferentially incorporated into the resulting glass, then the ratios {Px/Xtl}, {Ol/Xtl}, and {Ilm/Xtl} (where {Xtl} = {Px+Ol+Ilm}) are representative of the proportions of iron associated with those minerals in the rocks from which the regolith samples were derived. Figure 7 is a plot of those three ratios as a function of total iron content (as FeO), which is an indicator of the highland (FeO < 7 wt. %) versus mare (FeO >12 wt. %) nature of the soils. At one extreme, soils derived mainly from high-Ti mare basalt (Apollo 11 and some from Apollo 17) have the highest FeO concentrations (16–18%; Fig. 7) and ilmenite abundances (Table 2 and [14]). At the other extreme, the highland soils (Apollo 16 and Apollo 17 massif soils) are rich in plagioclase derived from anorthositic rocks, which leads to low total-FeO concentrations. In the highlands soils, most of the iron is contributed by mafic impact-melt breccias and, at Apollo 17, troctolites [33, 34]. Troctolite and the melt breccias from these two sites both have moderately high modal abundances of olivine and low abundances of ilmenite compared to mare basalt. Thus, the highland soils of Apollo 16 and 17 are distinguished by the highest {Ol/Xtl} and lowest {Ilm/Xtl} among the soils studied. Those soils from Apollo 17 that plot on a line between the mare and highlands extremes on Figure 7 (i.e., those with 10–12% FeO) are mixtures containing subequal amounts of mare and highland material; similar mare-highlands mixing trends are observed in the compositional data [34, 35].

In contrast to the highland soils of Apollos 16 and 17, the nominally highland soils of Apollo 14 were formed almost exclusively from mafic impact-melt breccias (10% FeO), but a variety with low modal abundance of olivine compared to those of Apollo 16 and 17. As a consequence, the Apollo 14 sample is richer in FeO (less "dilution" by plagioclase), and has lower {Ol/Xtl} and higher {Px/Xtl} than the highland soils of Apollos 16 and 17. Soils derived primarily from low-Ti mare basalt, such as those from Apollo 12 and 15, also derive most of their Fe from pyroxene and, thus, have high {Px/Xtl} and {Px/Ol} ratios, similar to Apollo 14 soil. However, because mare basalts have FeO concentrations twice as great as even the most mafic of highland impact-melt breccias, the soils of Apollo 12 and 14 are easily distinguished from those of Apollo 14 by their higher FeO concentrations.

A good example of the ability of Mössbauer mineralogy to distinguish mineralogy is Apollo 16 soil 67511, which is characterized by low {Ilm/Xtl} (~0.08) and, in contrast to other Apollo 16 soils, high {Px/Xtl} (~0.65) and intermediate {Ol/Xtl} (~0.26) (Table 2 and Figure 7). Among Apollo 16 soils, sample 67511 is also highly anomalous compositionally and mineralogically (from petrographic observations) [36, 37]. It contains a much lower abundance of mafic melt breccia and is instead dominated by crystalline material probably derived from a single pluton of noritic anorthosite [36]. Thus, Fe is carried mostly by low-Ca pyroxene resulting in a high {Px/Xtl}, similar to the soils of Apollo 12, 14, and 15. The apparent horizontal trends formed by these unrelated samples (i.e., {Px/Xtl} ~ 0.67 and {Ilm/Xtl} ~0.08) in Figures 7a and 7b is merely a reflection of their high {Px/Xtl}, closure (i.e., necessarily low {Ilm/Xtl} and {Ol/Xtl}), and a large variation in the ratio of plagioclase to Fe-bearing minerals among these diverse soils.

Figures 3, 6, and 8 show that Mössbauer mineralogy alone (i.e., without chemical or petrographic data) can easily distinguish soils from different Apollo landing sites, with respect to both mineralogy and mode of formation. High values of {Ol+Gl} (>70%) and low values of {Px/(Px+Ol)} (<0.15) separate volcanic ash from impact-derived regolith (Figure 3). Figure 8 is used to determine the mineralogy of impact-derived regoliths. For example, regoliths derived mostly from high-Ti mare basalts (Apollo 11 and

the valley floor at Apollo 17) have high values of both {Ilm/(Ilm+Ol)} and {Px/(Px+Ol)} and plot along the {Ilm}={Px} line. Regolith from the lunar highlands (Apollo 16 and Apollo 17 massifs) have low values of {Ilm/(Ilm+Ol)} (~ 0.10) and {Px/(Px+Ol)} (~ 0.50).

The linear, mare-highlands mixing trends defined by the Apollo 16 and 17 soils on Figure 7 break down on Figure 8 because there are actually two types of basaltic material (crystalline high-Ti basalt and volcanic ash) and several types of highlands materials (melt breccias, granulitic breccias, troctolitic anorthosites) [34, 35], each of which plot in different areas of the diagrams. The relative abundance of these various components in the regolith varies according to sample location at the site, which is geologically complex. Mineralogically, samples collected closest to the massifs (lowest abundance of mare basalt and pyroclastic glass) most closely resemble the Apollo 16 soils.

Mössbauer Mineralogy and Modal Petrography

For regolith samples, it is not possible to make direct comparisons between Mössbauer mineralogy (which is based on distribution of iron among specific iron-bearing phases in the <1 mm size fraction of soil) and conventional modal petrography, for which there is a large body of data [e.g., 12-14]. This is the case because the latter is based on the frequency of occurrence (often for a specific size fraction of soil) of different types of particles, many of which are complex assemblages that contain mineral components. For example, the five major categories used by Papike et al. [13] for their grain-count modal petrography are lithic fragments, mineral fragments, glass fragments, fused soil components, and miscellaneous. Lithic fragments and fused soil components both contain mineral grains in proportions not reported. Fused soil components contain unknown proportions of glass. The mineral fragments category does contain information about the proportions of minerals, but olivine and pyroxene are lumped into one category called "mafics." Similarly, the modal petrography of Heiken and McKay [12], which is based on the 90-150 μm size fraction of soil, has categories for particles (e.g., agglutinates and black glass) that are actually composites of glass and minerals.

The approach taken by Chambers et al. [38], who used thin sections of the 45–90 μm size fraction of soil, produces modal data that are more equivalent to Mössbauer mineralogy. They identified mineralogies (e.g., plagioclase, olivine, pyroxene, glass, and ilmenite) and then used x-ray/backscattered electron signal digital-imaging techniques to determine volume percentages. We have calculated values of {phase/Xtl} from these data by assuming values of 3.4, 3.8, and 4.7 g/cm^3 for densities [39-41] and 16.1, 27.0 and 44.2 wt. % for FeO concentrations in pyroxene, olivine, and ilmenite [e.g., 29-31], respectively, and compared them to the results from Mössbauer mineralogy in Table 4 for the only two soils analyzed in common. Considering that different grain-size fractions were analyzed and the concentration of FeO is highly variable in pyroxenes from high-Ti mare basalt, the agreement is reasonable, although there is a factor-of-two difference in the abundance of olivine obtained by the two techniques. In any event, we suggest that Mössbauer mineralogy is arguably the technique of choice for mineralogical characterization of lunar soils. If textural relationships between mineral phases or mode of occurrence (i.e., olivine crystal in a volcanic glass bead or a lithic fragment) are important, then modal petrography is more appropriate.

Metallic Iron and the Solar Wind

Because it lacks an atmosphere, the lunar surface is exposed to H, He^3, C, N, and other light elements from the solar wind. Because ions of these elements are implanted to a depth of only a few micrometers, the solar wind elements are concentrated in the finest grain-size fraction of regolith. They are also found in agglutinates, which are glassy, irregularly-shaped breccia particles formed largely from fine-grained material in the upper ~1 mm of the lunar regolith by impact of micrometeorites. Because the proportion of agglutinate particles in a regolith sample increases with the length of exposure of the sample to micrometeorite impact at the surface, the parameter "% agglutinates" is used as an index of surface exposure [12, 42]. The amount of metallic iron in the lunar regolith also increases with surface residence time. The metal is derived from the micrometeorites themselves as well as from reduction of lunar ferrous iron. The reduction occurs as a consequence of micrometeorite impact into regolith bearing hydrogen

supplied by the solar wind [e.g., 43]; the amount of metal formed is proportional both to the length of exposure (i.e., the amount of H) and the amount of ferrous iron available for reduction. The index of surface exposure based on metal formed by reduction is designated I_s/FeO, where I_s is the relative concentration of fine-grained metal as measured by ferromagnetic resonance (FMR) and FeO is the total concentration of iron [42, 44]. The high degree of correlation between I_s/FeO and the concentration of solar-wind-derived N [42, 45] is strong evidence for both the accumulation of metal from reduction of ferrous iron during surface exposure and the use of I_s/FeO as an index of surface exposure.

Housley et al. [46] reported a correlation between FMR data and metallic iron concentrations determined by Mössbauer spectroscopy. Their approach was to measure the "excess area" near zero velocity which they considered to result from the fine-grained metal formed from exposure-induced reduction of ferrous iron. The excess area, ΔA, is defined as the difference obtained by subtracting the area in the Mössbauer spectrum between 1.08 and 3.28 mm/s from the area in the interval between 0.92 and 1.08 mm/s, where 1.08 mm/s is the IS for ilmenite. The rationale was that all doublet species (olivine, pyroxene, glass, and ilmenite) and the sextet from α-Fe^0 would contribute equally to both areas and sum to zero, leaving the contribution from fine-grained metal [8, 46]. If this interpretation of ΔA is valid, it should correspond to our values of {np-Fe^0} in Table 2. However, ΔA is not equal to zero for the metallic iron sextet because the centers of peaks 3 and 4 are both less than 1.08 mm/s. Thus, ΔA includes contributions from both {np-Fe^0} and {α-Fe^0}. This oversight by [46] does not negate their correlation between Mössbauer and FMR data, but it does call into question their interpretations regarding the range of metal particle diameters to which the techniques are sensitive.

Values of {α-Fe^0}, {np-Fe^0}, and I_s/FeO are measures of the proportion of iron that is present as metallic iron for different populations of metallic iron particles. According to the arguments of [46], the population of metal particles that contributes to I_s/FeO is the same one that contributes to {np-Fe^0}, although this may not be exactly the case as discussed above. In Figure 9, {np-Fe^0} is plotted as a function

of I_s/FeO. Although considerable scatter is present in the data, it is apparent that values of {np-Fe^0} can be used as approximate indicators of regolith maturity. It is possible that the correlation of {np-Fe^0} with I_s/FeO would be improved under experimental conditions where the blank contribution is not present.

It should be noted that a portion of the {α-Fe^0} component of the regolith is not related to surface exposure, but is contributed by the rocks of which the soil is composed. This is especially true at Apollo 16, where mafic impact-melt breccias, which constitute 30% of the regolith, contain 1–2 % Fe-Ni metal because the breccias were formed by impact of large, metal-rich meteorites [33]. As a consequence, Apollo 16 soils have the greatest average values of {α-Fe^0} among Apollo soils (Table 2, excluding anomalous 67511, which contains only a small melt breccia component).

Mössbauer Mineralogy and Lunar Exploration

It is evident from the above discussion that Mössbauer spectrometers can be used as powerful tools for robotic, in situ mineralogical exploration of the Moon. Samples of rock and regolith that are mineralogically (from Figures 3 and 7–9) and/or chemically (from total resonant absorption) different from previously sampled materials can be identified and characterized. In addition to acquiring basic mineralogical data, the instrument data can be used to select representative samples for return to a lunar base or to the Earth for other kinds of analyses (e.g., petrography and age dating). The effectiveness of the instrument can be enhanced when used in conjunction with other instruments, such as a Raman spectrometer, that provide complimentary data [47]. Establishment of a human presence on the Moon will undoubtedly entail utilization of indigenous resources, including production of oxygen by reduction of silicate and oxide (especially ilmenite) phases [e.g., 48, 49]. Because oxygen yield from lunar soils is related primarily to the total Fe content and secondarily to the mineralogy of iron-bearing phases [49], Mössbauer mineralogy can be used to "assay" regolith to find the best "ore" for oxygen production. Knowing the distribution of Ti among carrier phases is critical for proper interpretation of spectral

reflectance data obtained remotely [50]. Ice has been postulated to exist in permanently shadowed regions near the south pole of the Moon [51, 52]. Micrometeorite impact into mixtures of ice and ferrous-bearing material would likely produce an assembly of phases (possibly ferric-bearing phases like magnetite) not previously sampled on the Moon. Detection of these phases by a Mössbauer spectrometer would provide evidence for the current or past presence of ice. Ice sequestered at depth could have a ferric-bearing manifestation detectable at the surface by a Mössbauer spectrometer.

All the Mössbauer data on lunar materials discussed here are absorption spectra resulting from the transmission geometry (samples are located between the ^{57}Co source and detector) of the instrument. This is not a preferred geometry for planetary exploration because a mechanism is required to prepare a sufficiently thin sample and place it between source and detector. Backscatter geometry (source and detector are on the same side of a sample, which results in emission Mössbauer spectra) is better for planetary applications because no sample preparation is required. The source-detector assembly is simply placed, e.g., by a robotic arm, against a soil or rock sample for analysis. Alternatively, the source-detector assembly could be incorporated into the body of a rover or lander with a solid window that permits passage of 14.4 keV γ-rays (e.g., Be metal). In a vertical orientation (i.e., source γ-rays emanating vertically and with a horizontal window), samples could be placed on and removed from the window by a robotic arm or some other mechanism. Whatever deployment mechanism is used, additional laboratory measurements will be necessary to determine if the quantitative relationships in Figures 3 and 7–9 are sensitive to measurement geometry. While we do not anticipate significant differences, the worst-case scenario is reacquisition of all the Mössbauer spectra in backscatter geometry. A comparison of transmission (laboratory instrument) and backscatter (flight-prototype instrument developed at the NASA Johnson Space Center) Mössbauer spectra for regolith sample 71131 is shown in Figure 10.

Additional laboratory measurements are also needed for lunar applications of Mössbauer mineralogy. Regolith samples from Apollo 12, 14, and 15 missions are not well represented in Figures 3 through 9, and several lunar meteorites represent regoliths significantly different from those sampled by the

Apollo missions [e.g., 53]. Lunar rocks have not been studied in a systematic way. These measurements will give a complete picture of the Mössbauer mineralogy of the lunar surface for which we presently have samples and provide a basis for identification of new types of rocks and regolith. The temperature range for the lunar surface is 150 to 520 K, so it will be necessary to understand the Mössbauer spectra of lunar materials at those temperatures. Finally, because of the potential for size sorting of regolith on the Moon, the Mössbauer mineralogy of lunar regolith samples with respect to size fraction (particularly the finest fractions) should be investigated.

References

[1] COMPLEX (Committee on Lunar and Planetary Exploration), *Strategy for Exploration of the Inner Planets: 1977-1987* (Space Science Board, National Academy of Sciences 1978).

[2] D.G. Agresti, R.V. Morris, E.L. Wills, T.D. Shelfer, M.M. Pimperl, M.-H. Shen, B.C. Clark and B.D. Ramsey, Hyp. Int. 72 (1992) 285.

[3] G. Klingelhöfer, B. Fegley Jr., R.V. Morris, E. Kankeleit, P. Held and E.P.O. Evlanov, Planet. Space Sci. 44 (1996) 1277.

[4] P. Gay, G.M. Bancroft and M.G. Brown, Proc. Lunar Planet. Sci. Conf. 11 (1970) 481.

[5] T.C. Gibb, R. Greatrex, N.N. Greenwood and M.H. Battey, Proc. Lunar Planet. Sci. Conf. 3rd (1972) 2479.

[6] C.L. Herzenberg and D.L. Riley, Proc. Lunar Planet. Sci. Conf 1st (1970) 2221.

[7] R.M. Housley, M. Blander, M. Abdel-Gawad, R.W. Grant and A.H. Muir Jr., Proc. Lunar Sci. Conf. 11th (1970) 2251.

[8] R.M. Housley, R.W. Grant, A.H. Muir Jr., M. Blander and M. Abdel-Gawad, Proc. Lunar Planet. Sci. Conf. 2nd (1971) 2125.

[9] R.M. Housley, R.W. Grant and N.E. Paton, Proc. Lunar Sci. Conf. 4th (1973) 2373.

[10] G.P. Huffman, F.C. Schwerer and R.M. Fisher, Proc. Lunar Planet. Sci. Conf. 5th (1974) 2779.

[11] S. Mitra, Applied Mössbauer Spectroscopy, Theory and Practice for Geochemists and Archaeologists (Permagon Press, New York, 1992).

[12] G. Heiken and D.S. McKay, Proc. Lunar Planet. Sci. Conf. 5th (1974) 843.

[13] J.J. Papike, S.B. Simon and J.C. Laul, Rev. Geophys. Space Phys. 20 (1982) 761.

[14] G.H. Heiken, D.T. Vaniman and B.M. French, *Lunar Sourcebook, A User's Guide to the Moon* (Cambridge University Press, New York, 1991) p. 736.

[15] S.R. Taylor, *Lunar Science: A Post-Apollo View* (Pergamon Press, New York, 1975) p. 372.

[16] S.R. Taylor, *Planetary Science: A Lunar Perspective* (Lunar and Planetary Institute, Houston, 1982) p. 481.

[17] S. Margulies and J.R. Ehrman, Nucl. Inst. Meth. 12 (1961) 131.

[18] D.G. Rancourt, A.M. McDonald, A.E. Lalonde and J.Y. Ping, Am. Mineral. (1993) 1.

[19] D.L. Williamson, T.W. Guettinger and D.W. Dickerhoof, In: *Mössbauer Spectroscopy and Its Chemical Applications*, Eds J.G. Stevens and G.K. Shenoy (American Chemical Society, Washington, D. C., 1981) p. 178.

[20] J. Graf, *Lunar Soils Grain Size Catalog* (NASA Reference Publication 1265, NASA, Washington. D.C., 1993)

[21] E. De Grave and A. Van Alboom, Phys. Chem. Minerals 18 (1991) 337.

[22] G. Heiken and D.S. McKay, Proc. Lunar Planet. Sci. Conf. 9th (1978) 1933.

[23] J. Arndt, W.v. Englehardt, I. Gonzalez-Cabeza, and B. Meier, Proc. Lunar Planet. Sci. Conf. 15th (1984) C255-C232.

[24] G. Ryder and M.D. Norman, *Catalog of Apollo 16 Rocks, Part 3. 67015 - 69965* (NASA Johnson Space Center, JSC 16904, Houston, TX, 1980).

[25] C.R. Neal and L.A. Taylor, *Catalog of Apollo 17 Rocks, Volume 2 - Central Valley, Part 1* (NASA Johnson Space Center, JSC #26088, Houston, TX, 1993).

[26] C.R. Neal and L.A. Taylor, *Catalog of Apollo 17 Rocks, Volume 3 - Central Valley, Part 2* (NASA Johnson Space Center, JSC #26088, Houston, TX, 1993).

[27] C. Meyer, *Catalog of Apollo 17 Rocks, Volume 4 - North Massif* (NASA Johnson Space Center, JSC #26088, Houston, TX, 1994).

[28] F. Horz and M. Cintala, Meteorit. Planet. Sci. 32 (1997) 179.

[29] J.W. Delano, Proc. Lunar Planet. Sci. Conf. 6th (1975) 15.

[30] R.F. Dymek, A.L. Albee, and A.A. Chodos, Proc. Lunar Planet. Sci. Conf. 6th (1975) 49.

[31] W.I. Ridley, Proc. Lunar Planet. Sci. Conf. 6th (1975) 131.

[32] R.V. Morris, Proc. Lunar Planet. Sci. Conf. 11th (1980) 1697.

[33] R.L. Korotev, Meteorit. Planet. Sci. 32 (1997) 447.

[34] B.L. Jolliff, K.M. Rockow, R.L. Korotev, and L.A. Haskin, Meteorit. Planet. Sci. 31 (1996) 116.

[35] R.L. Korotev and D.T. Kremser, Proc. Lunar Planet. Sci. 22nd (1992) 275.

[36] B.L. Jolliff and L.A. Haskin L. A., Geochim. Cosmochim. Acta 59 (1995) 2345.

[37] R.L. Korotev, Meteorit. Planet. Sci. 31 (1996) 403–412.

[38] J.G. Chambers, L.A. Taylor, A. Patchen and D.S. McKay, J. Geophys. Res. 100 (1995) 14391,401.

[39] W.A. Deer, R.A. Howie, and J. Zussman, *Rock-Forming Minerals, Vol. 5, Non-Silicates*, (Longman, New York, 1962) p. 371.

[40] W.A. Deer, R.A. Howie, and J. Zussman, *Rock-Forming Minerals, Vol. 2A, Single-Chain Silicates*, (Longman, New York, 1978) p. 668.

[41] W.A. Deer, R.A. Howie, and J. Zussman, *Rock-Forming Minerals, Vol. 1A, Orthosilicates*, (Longman, New York, 1982) p. 919.

[42] R.V. Morris, Proc. Lunar Sci. Conf. 7th (1976) 315.

[43] R.M. Housley, E.H. Cirlin and R.W. Grant, Proc. Lunar Planet. Sci. Conf. 4th (1973) 2729.

[44] R.V. Morris, Proc. Lunar Planet. Sci. Conf. 9th (1978) 1827.

[45] R.V. Morris, R.L. Korotev and H.V. Lauer Jr., Proc. Lunar Planet. Sci. Conf. 19th (1989) 269.

[46] R.M. Housley, E.H. Cirlin, N.E. Paton and I.B. Goldberg, Proc. Lunar Sci. Conf. 5th (1974) 2623.

[47] L.A. Haskin, A. Wang, K.M. Rockow, B.J. Jolliff, R.L. Korotev, and K.M. Viskupic, J. Geophys. Res. 102 (1997) 19,293.

[48] L.A. Taylor L. A. and D.W. Carrier III, In *Resources of Near-Earth Space*, (J. S. Lewis, M. S. Matthews, and M. L. Guerrieri, eds., University of Arizona Press, Tucson, 1993) 69.

[49] C.C. Allen, R.V. Morris and D.S. McKay, J. Geophys. Res. 99 (1994) 23,173.

[50] D.T. Blewett, P.G. Lucey, B.R. Hawke, and B. J. Jolliff, J. Geophys. Res. 102 (1997) 16,319.

[51] J. R. Arnold, J. Geophys. Res. 84 (1979) 5659.

[52] S. Nozette, C.L. Lichtengerg, P. Spudis, R. Bonner, W. Ort, E.Malaret, M. Robinson, and E.M. Shoemaker, Science 274 (1996) 1495.

[53] R.L. Korotev, B.J. Jolliff, and K.M. Rockow, Meteorit. Planet. Sci. 31 (1996) 909.

Figure Captions

Figure 1. Mössbauer spectra for impact-derived regolith. Locations of peaks for individual phases are indicated by the stick diagram. Ilmenite and especially pyroxene are the dominant crystalline phases in mare samples, and pyroxene and olivine are the dominant crystalline phases in highland samples.

Figure 2. Mössbauer spectra for volcanic-ash regolith. Locations of peaks for individual phases are indicated by the stick diagram. The dominant phases in the upper two samples are glass and olivine, and the dominant phases for the bottom sample are olivine and pyroxene.

Figure 3. Plot of {Ol+Gl} versus {Px/(Px+Ol)}. Volcanic-ash regolith, which have high concentrations of glass and/or olivine, plots in region in the upper left corner. Rock powders, which have low amounts of glass, have high values of {Px/(Px+Ol)}. Impact-derived regolith generally has intermediate values of {Ol+Gl} and {Px/(Px+Ol)}.

Figure 4. Measured versus calculated {Ilm}. For Model 1 (open squares), values of {Ilm} were calculated assuming all Ti is present as stiochiometric ilmenite. For Model 2 (filled circles), values of {Ilm} were calculated by accounting for deviations from stoichiometry and the presence of Ti in glass and pyroxene.

Figure 5. Measured versus calculated {tot-Fe^0}. Calculated values of {tot-Fe^0} were obtained from Fe^0 concentrations determined magnetically and from total Fe concentrations determined from chemical analyses. The correlation coefficient (R^2) from a linear least squares fit constrained to pass through the origin is 0.92.

Figure 6. Total resonant absorption area versus FeO. FeO is the total iron concentration determined by chemical analyses. The correlation coefficient (R^2) from a linear least squares fit constrained to pass through the origin is 0.83.

Figure 7. Plots of (a) {Ilm/Xtl}, (b) {Px/Xtl}, and (c) {Ol/Xtl} (where {Xtl}={Px+Ol+Ilm}) versus total FeO concentrations determined by chemical analyses for impact-derived soils. Soils having <7% FeO are derived mostly from the lunar highlands and soils having >12% FeO are derived mostly from

lunar maria. Soils having intermediate FeO concentrations are highland-mare mixtures and/or mafic basin ejecta.

Figure 8. Plots of (a) {Ilm/(Ilm+Ol)} versus {Px/(Px+Ol)} and {Ol/Xtl} versus {Px/Xtl} for impact-derived regolith. Mössbauer mineralogy readily distinguishes mineralogical differences among the smaples.

Figure 9. Plot of {np-Fe^0} versus the regolith maturity index I_s/FeO. The correlation coefficient (R^2) from a linear least squares fit constrained to pass through the origin is 0.91.

Figure 10. Transmission and backscatter Mössbauer spectra for Apollo 17 mare soil 71131. Backscatter spectrum was obtained with a flight-prototype instrument developed at the Johnson Space Center.

Table 1. Components and Mössbauer parameters (293 K) for a generic lunar soil.

Component	IS (mm/s)	QS (mm/s)	B_{hf} (T)	Line Numbers	W (mm/s)	Shape
Olivine {Ol} Fe^{2+}	1.147	2.961		1 & 2	0.300	0.000
Pyroxene {Px} Fe^{2+}						
M2 Site	1.128	2.074		1 & 2	0.350	0.000
M1 Site	1.148	2.474		1 & 2	0.350	0.000
Glass {Gl} Fe^{2+}	1.076	2.074		1 & 2	0.749	0.839
					0.873	0.732
Ilmenite {Ilm} Fe^{2+}	1.075	0.688		1 & 2	0.330	0.000
{α-Fe^0}	0.015	-0.020	33.01	1 & 6	0.400	0.000
				2 & 5	0.360	0.000
				3 & 4	0.320	0.000
{np-Fe^0}	0.218				0.540	0.000

Notes: IS=isomer shift; QS=quadrupole shift; B_{hf}=hyperfine field; W=linewidth. Lines are numbered from lowest to highest velocity. Shape is fraction Gaussian of a mixed Gaussian-Lorentzian lineshape function.

Table 2. Mössbauer mineralogy of lunar samples. Numbers following the comma in the sample designation are subsplit designations issued by the lunar sample curator.

Sample	{Ol} (%)	{Px} (%)	{PxM2} (%)	{PxM1} (%)	{Gl} (%)	{Ilm} (%)	{α-Fe^0} (%)	{np-Fe^0} (%)
Lunar regolith samples, <1 mm size fraction								
10084,853	3	19	14	5	50	19	6	3
12032,24	17	48	34	14	26	5	3	1
12044,11	15	35	25	10	38	5	3	4
14148,23	10	38	32	6	37	5	4	4
15013,94	15	37	26	11	37	4	3	4
15421,64	14	2	2	0	79	2	1	2
60501,89	25	27	23	4	33	3	8	5
62241,77	23	23	20	3	39	3	7	6
66031,8	24	25	21	4	34	3	7	7
67511,1	30	65	57	8	0	3	0	2
68121,3	25	31	27	4	28	3	8	4
69921,11	24	27	23	4	32	3	8	7
70251,1	10	23	18	5	41	21	3	2
71061,12	14	24	18	6	38	23	1	1
71131,4	9	27	21	6	36	23	3	2
72131,4	13	19	15	4	43	18	4	3
72161,61	16	12	11	1	51	12	6	4
72241,2	25	36	32	4	27	5	4	3
73131,2	37	43	36	7	14	4	2	0
73151,4	27	31	27	4	30	5	4	3
73241,20	31	35	29	6	23	7	2	2
74001,119	36	0	0	0	46	18	0	0
74111,1	25	30	25	4	31	10	3	2
74220,84	15	0	0	0	76	8	0	0
76031,4	19	22	18	4	39	12	4	3
76131,4	19	25	20	5	37	12	4	3
78461,51	13	21	17	4	44	13	5	4
Lunar regolith sample, <20 μm size fraction								
10084,853	4	12	9	3	45	23	9	7
Lunar rock samples (powders)								
67215,8	45	52	45	7	2	2	0	0
70035,157	2	47	35	12	13	36	0	2
75075,174	1	47	35	12	13	36	0	2
76015,186	30	60	46	14	5	7	0	0
77017,175	38	59	45	14	2	1	1	0
77135,191	43	49	40	9	4	2	2	0
Uncertainty	2	3	3	2	3	2	1	1

Table 3. Mössbauer parameters (293 K) for olivine, pyroxene (M2 site), and ilmenite from lunar regolith and rock samples.

Sample	Olivine		Pyroxene (M2)		Ilmentite	
	IS (mm/s)	QS (mm/s)	IS (mm/s)	QS (mm/s)	IS (mm/s)	QS (mm/s)
10084,853			1.123	1.950	1.068	0.689
12032,24			1.153	2.034		
12044,11			1.151	2.031		
14148,23			1.140	2.113		
15013,94			1.149	2.035		
60501,89	1.143	2.932	1.121	2.077		
62241,77	1.159	2.972	1.139	2.140		
66031,8	1.142	2.988	1.098	2.158		
67511,1	1.146	2.951	1.129	2.107		
68121.26	1.142	2.992	1.116	2.153		
69921,11	1.147	2.990	1.100	2.162		
70251,1			1.134	1.983	1.072	0.684
71061,12			1.137	1.974	1.073	0.688
71131,8			1.134	1.985	1.074	0.687
72131,4			1.132	1.987	1.073	0.690
72161,61			1.158	2.090		
72241,2	1.143	2.933	1.130	2.058		
73131,2	1.141	2.941	1.136	2.050		
73151,4	1.140	2.931	1.130	2.061		
73241,20	1.159	2.985	1.156	2.102		
74001,119	1.159	2.977				
74111,1	1.158	2.981	1.134	2.040		
76031,4	1.140	2.940	1.124	2.029		
76131,4	1.158	2.988	1.156	2.093		
78461,51			1.127	2.025		
Average	1.147	2.961	1.128	2.074	1.075	0.688
Std. Dev.	0.009	0.026	0.026	0.059	0.009	0.014
Lunar rock samples (powders)						
67215,8	1.145	2.964	1.138	2.110		
67511,1	1.146	2.950	1.129	2.106		
70035,157			1.148	2.056	1.094	0.687
75075,174			1.151	2.041	1.094	0.690
76015,186	1.154	3.015	1.151	2.100		
77017,175	1.153	2.984	1.147	2.090		
77135,191	1.151	3.017	1.149	2.106		
Average	1.148	2.970	1.132	2.077	1.080	0.687
Std. Dev.	0.008	0.032	0.025	0.055	0.012	0.012

Table 4. Comparison of results from modal petrology and Mössbauer mineralogy for relative abundances of iron in olivine, pyroxene, and ilmenite.

	Mode (volume %)	{Phase/Xtl} (atom %)	
		Mode	Mössbauer
	CT&P*	CT&P*	This Study
Regolith sample 71061			
Size Fraction	45-90 μm	45-90 μm	<1 mm
Olivine	9.8	11	23
Pyroxene	66.9	39	39
Ilmenite	23.3	51	38
Regolith sample 10084			
Size Fraction	45-90 μm	45-90 μm	<1 mm
Olivine	3.2	4	7
Pyroxene	80.6	54	46
Ilmenite	16.2	42	47

Chambers et al. [38]

Fig. 1, Morris et al. 1997, Moss Min Moon

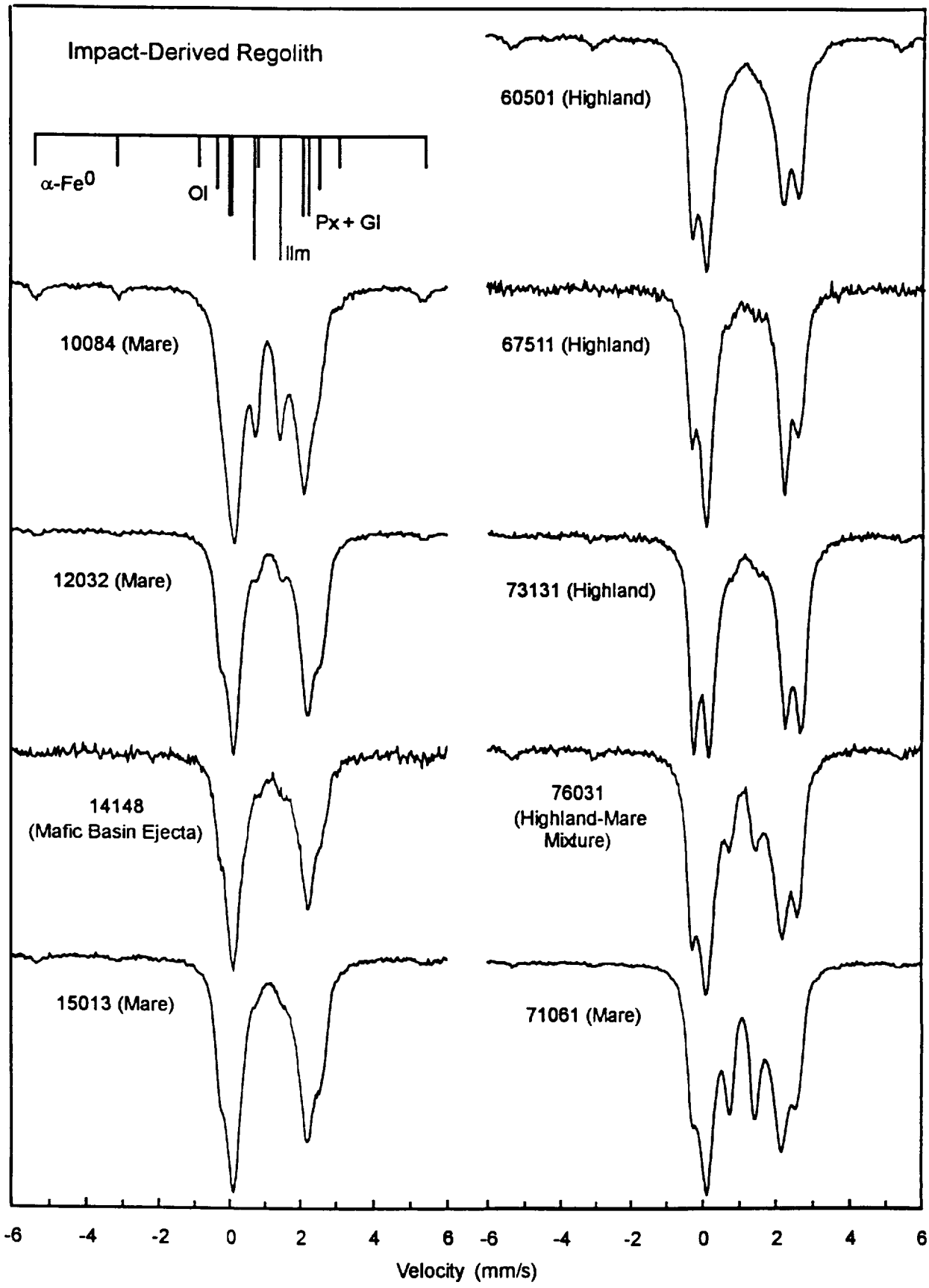

Fig. 2, Morris et al. 1997, Moss Min Moon

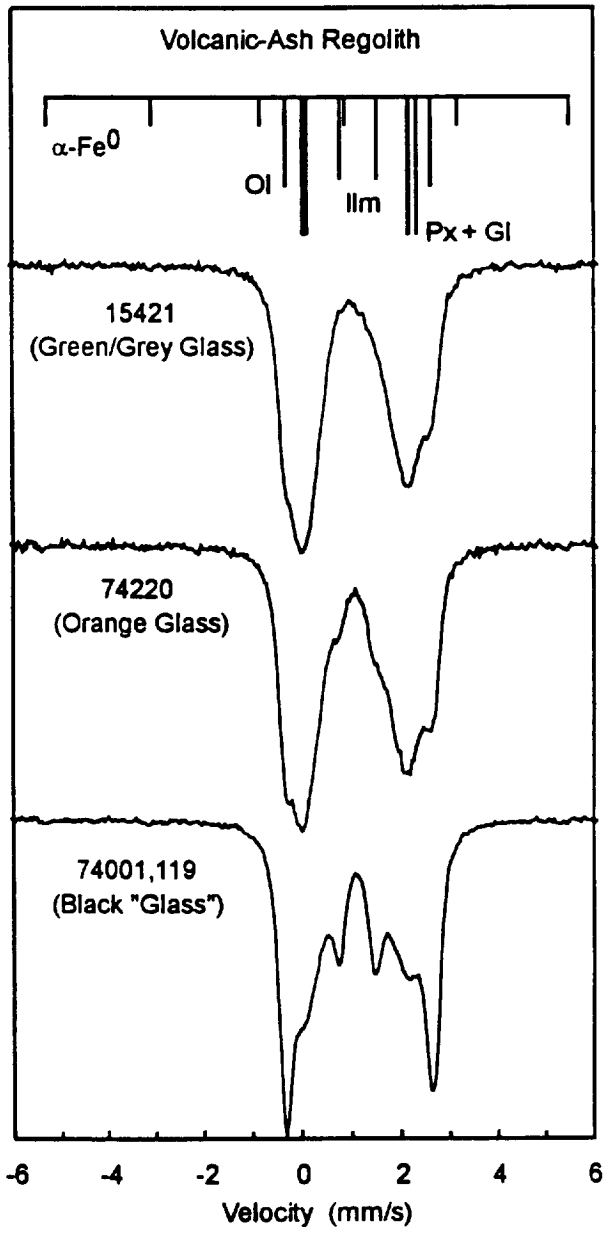

Fig. 3, Morris et al. 1997, Moss Min Moon

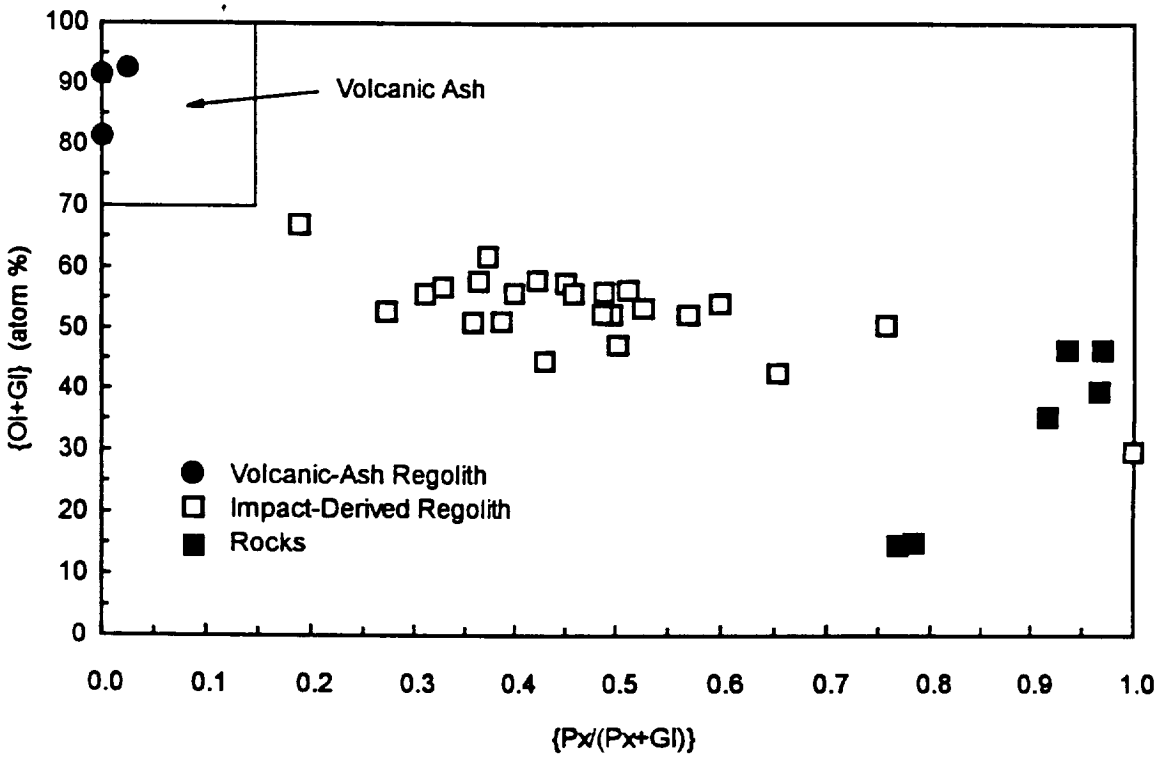

Fig. 4, Morris et al. 1997, Moss Min Moon

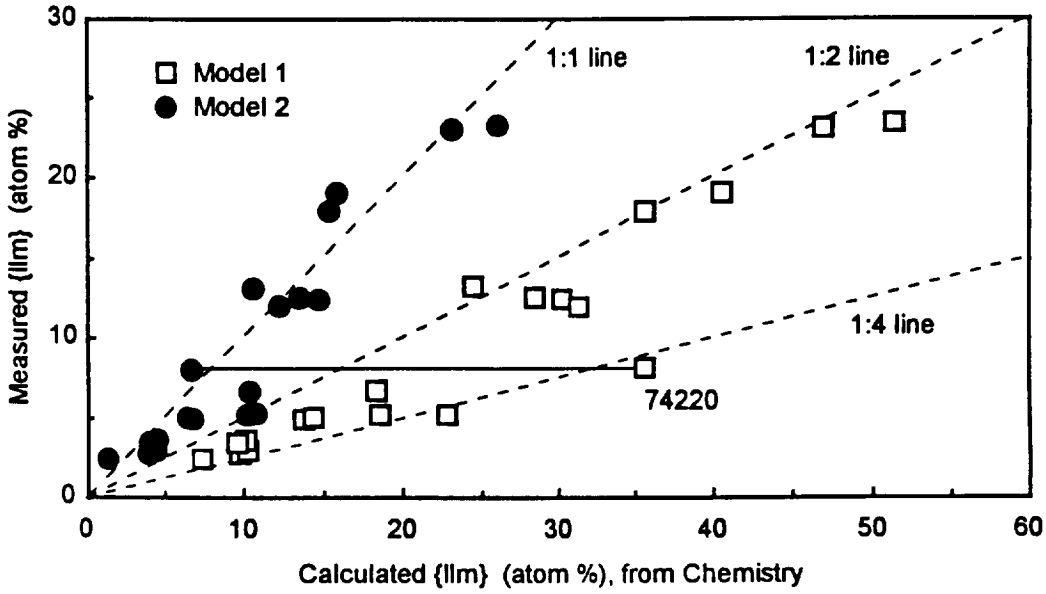

Fig. 5, Morris et al. 1997, Moss Min Moon

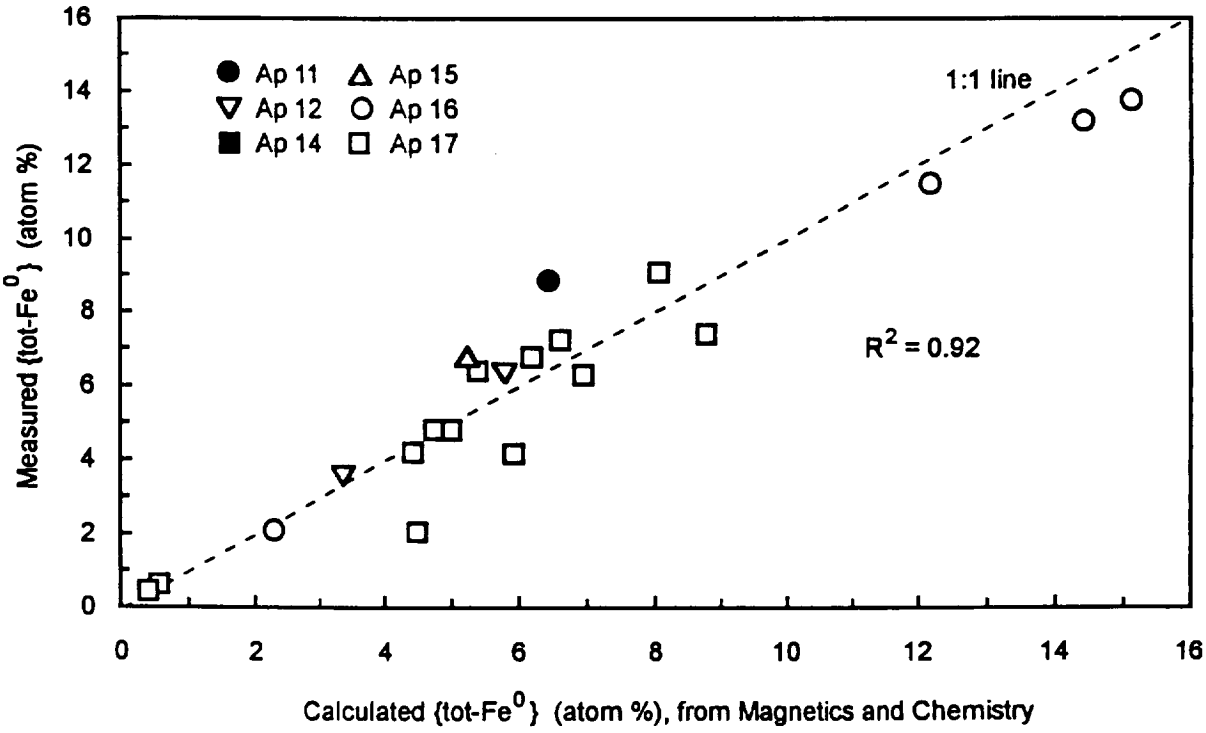

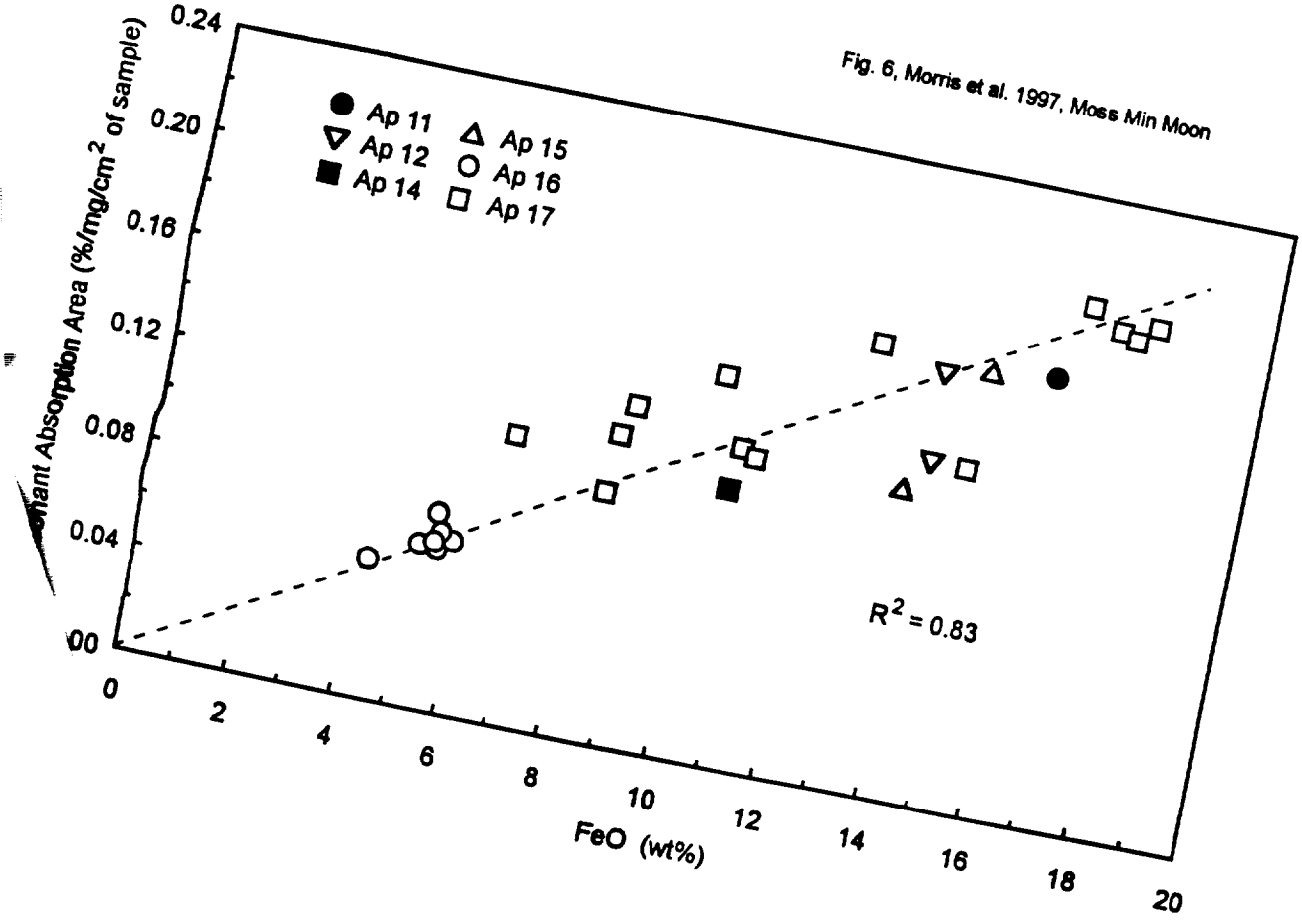
Fig. 6, Morris et al. 1997, Moss Min Moon
Ap 11
Ap 15
Ap 12
Ap 16
Ap 14
Ap 17
$R^2 = 0.83$
Glant Absorption Area (%/mg/cm^2 of sample)
0.24
0.20
0.16
0.12
0.08
0.04
00
0
2
4
6
8
10
12
14
16
18
20
FeO (wt%)

Fig. 7, Morris et al. 1997, Moss Min Moon

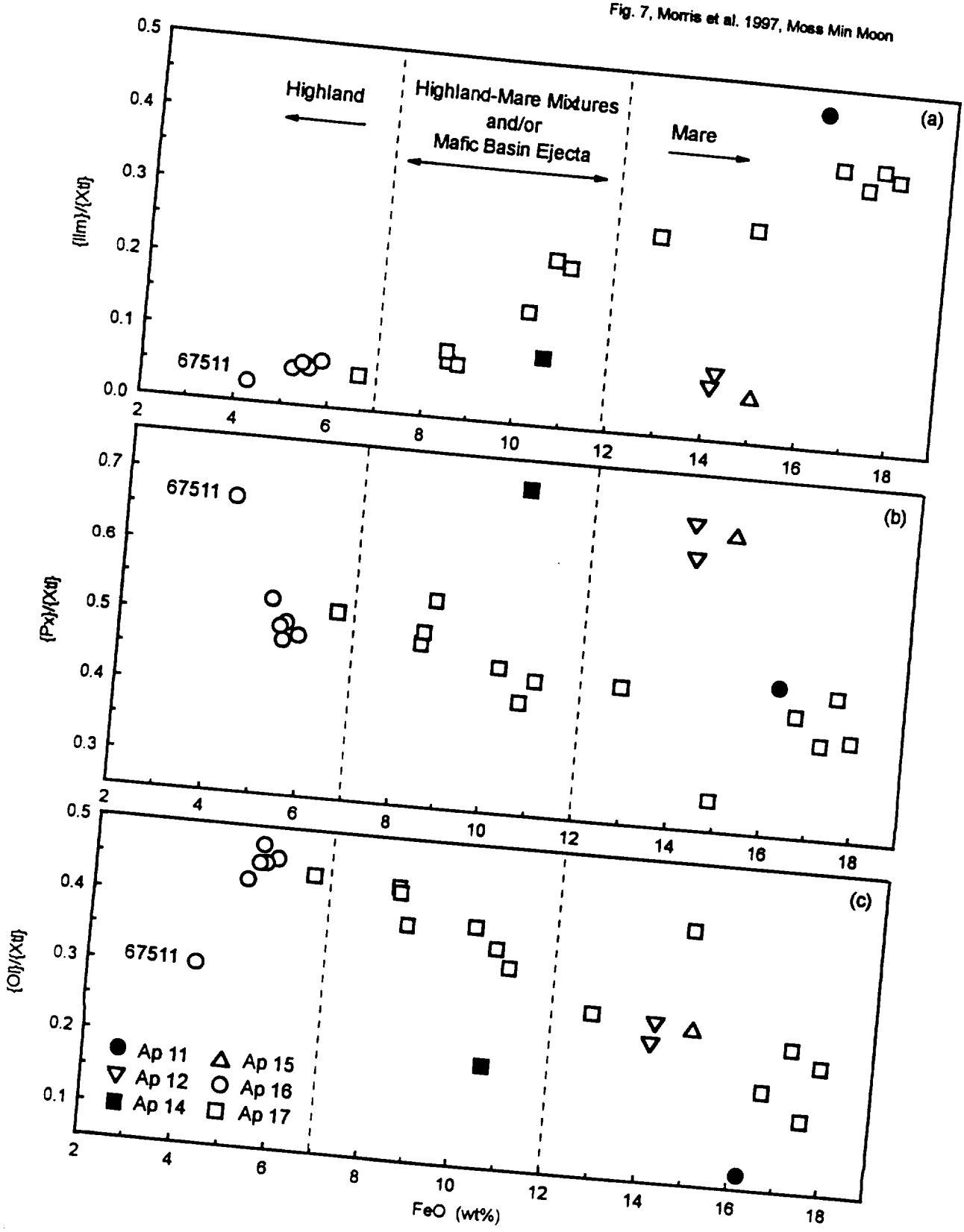

Fig. 8, Morris et al. 1997, Moss Min Moon

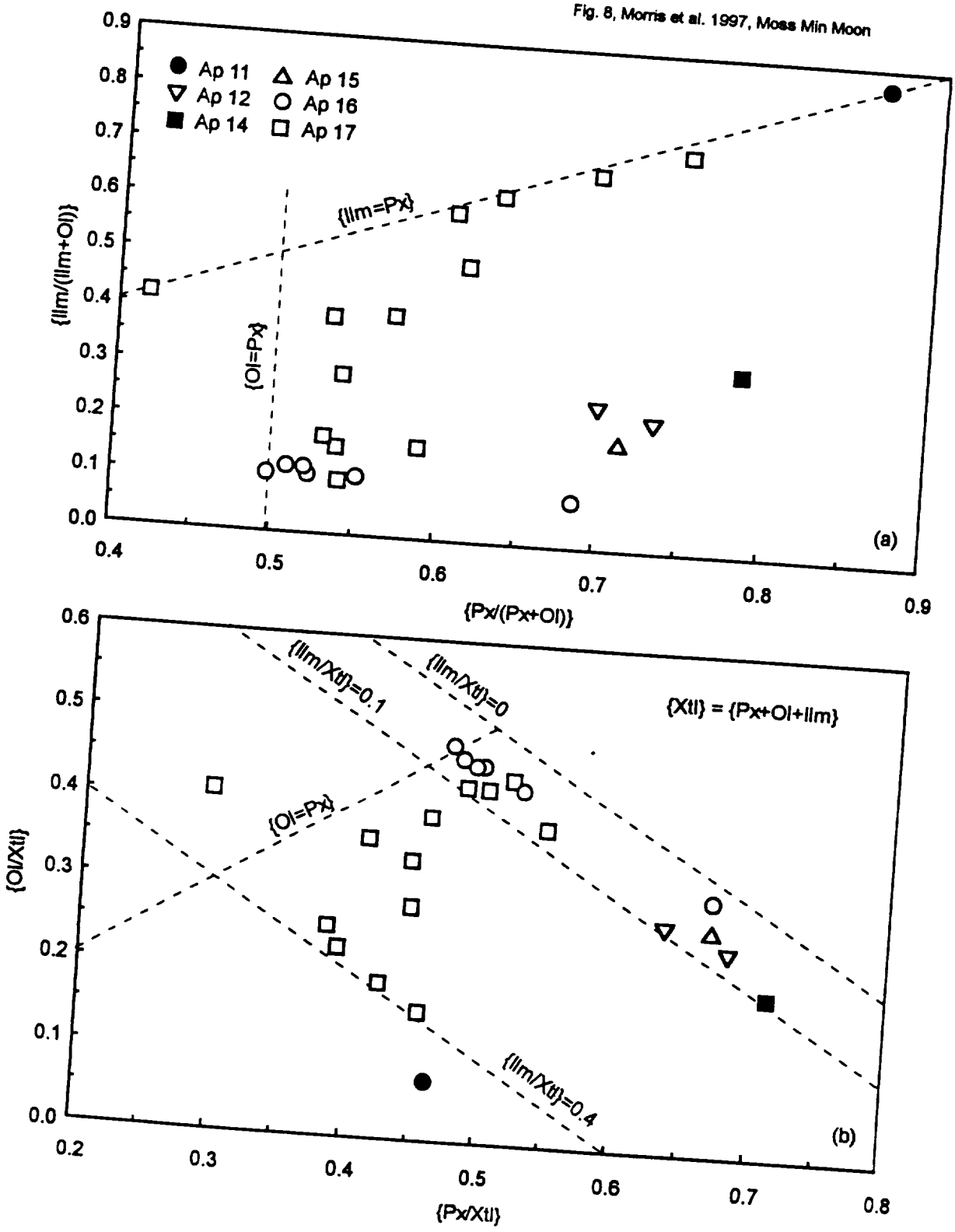

Fig. 9, Morris et al. 1997, Moss Min Moon

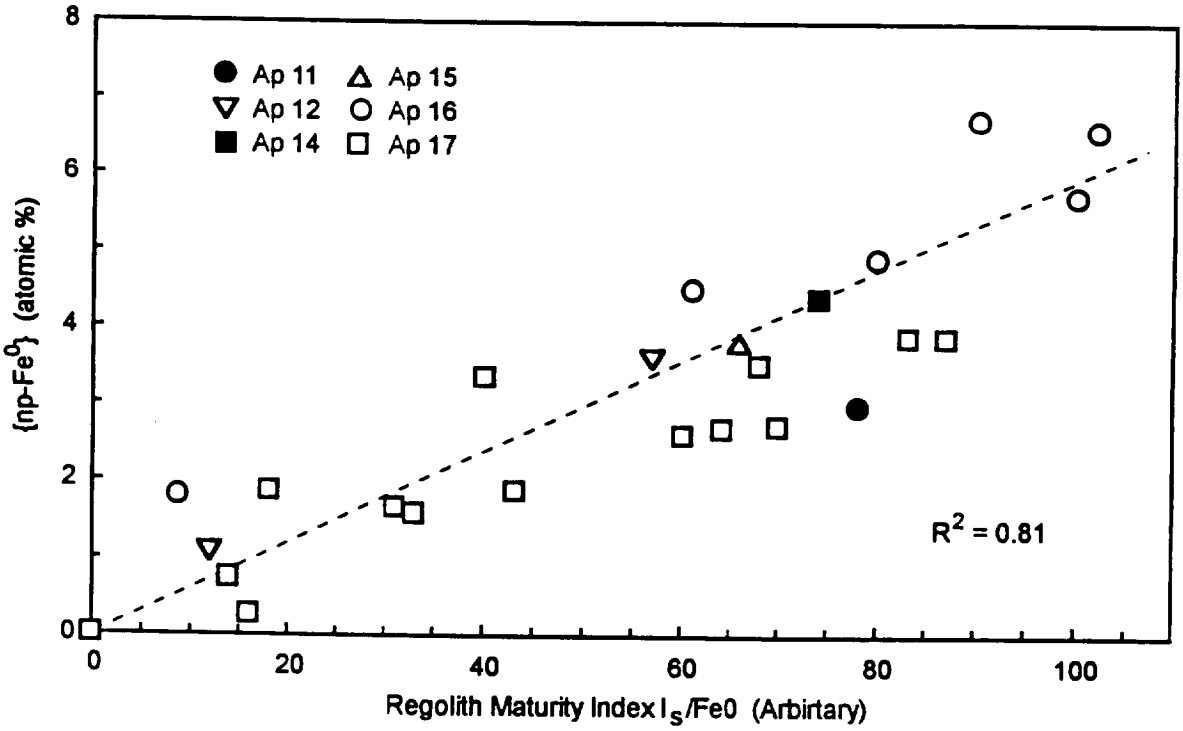

Fig. 10, Morris et al. 1997, Moss Min Moon